Stand-alone Heartbeat Detection in Multidimensional Mechanocardiograms

Matti Kaisti*, Mojtaba Jafari Tadi, Olli Lahdenoja, Tero Hurnanen, Antti Saraste, Mikko Pänkäälä and Tero Koivisto

***Abstract*—We describe a home health monitoring solution with cardiac beat-to-beat detection using accelerometer and gyroscope signal fusion. The proposed method measures both the precordial translational and rotational motions of the chest using miniaturized inertial sensors. The algorithm removes motion artefacts, selects the best axis from multi-axial accelerometric and gyroscopic signals and detects the location of beats using two detection principles based on i) the signal envelope and ii) signal morphology. We consider the beat-to-beat detection accuracy, estimate the heart rate and compare the detection performance between the sensor modalities in two study groups: i) healthy subjects and ii) heart disease patients. The average true and positive prediction rates of beat detection were 99.9% and 99.6% for the healthy subjects and up to 95.9% and 95.3% for the heart disease patients, respectively. Although high-accuracy beat detection was achieved for the heart disease patients, location matching in these patients was found to be less accurate compared to that of the healthy subjects. The average root mean square error (RMSE) between the mechanical and ECG interbeat intervals was 5.6 ms for the healthy patients; this error increased approximately ten-fold for the heart disease patients. Similarly, the RMSE for the averaged heart rate estimation showed about a ten-fold difference at 1.05 beats per minute (bpm) for the heart disease patients. The used sensor modalities are found in many electronic devices, such as smartphones and wearable technologies and the method provides a step towards ubiquitous cardiac monitoring.**

Keywords*—sensor fusion, beat-to-beat detection, wearable technology, accelerometer, gyroscope, seismocardiography, mechanocardiography

I. Introduction

PORTABLE devices for the home monitoring of cardiac health are expected to witness substantial growth in coming years. The increasing incidence of cardiovascular disease, the increase in geriatric populations and the demand for independent living are driving the growth of remote monitoring device markets [1]. Electrocardiography (ECG) is still the most widely used diagnostics tool in hospitals and at home. The measurement equipment for ECG, however, is not readily available for most patients, so they must acquire it and learn how to use it. An alternative rhythm management method, mechanocardiography (MCG), is based on measuring the mechanical motion induced by the heart [2]. Today, the sensors suited for this purpose – accelerometers and gyroscopes – are integrated into most smartphones and are available for most people. Combined with their ease of use, these devices have potential as a low cost home health monitoring solution.

Current wearable/handheld cardiac monitors can be divided into three groups. Monitors in the first group, such as ECG and impedance cardiography (ICG), measure electrical signals produced by heart's activity. The second group comprises methods that measure volumetric blood pressure variations using optical sensors, such as those in photoplethysmography (PPG), which are placed on fingertips, toes, earlobes, wrists and the face [3]. The third group includes mechanical cardiac monitoring, such as ballistocardiography (BCG), which detects changes in body recoil forces in response to blood ejection from the aorta to the vascular tree [4], [5]. Seismocardiography (SCG), which measures positional movements of the chest wall due to precordial vibrations [6], [7], also belongs to the third group. A complementary measurement technique to SCG has emerged: gyrocardiography (GCG) [8]. With the latest technological developments, these sensors have reasonable power consumption and high performance. Gyroscopes have higher tolerance to noise [9], and the obtained waveforms remain more monomorphic and stationary than they do in seismocardiograms.

In Fig. 1 typical waveforms from both accelerometer and gyroscope signals are presented. It is believed that the pulse waveform of a seismocardiogram reflects physiological events, such as mitral valve closure (MC), aortic opening (AO) and closure (AC), as well as mitral opening (MO) [7], [10], whereas GCG indicates myocardial deformation parameters and represents physiological phenomena, such as valvular opening and closure points and systolic–diastolic tissue velocities [8].

Smartphone mechanocardiography (sMCG) is a key application for the developed method as it is fully ECG-independent and requires neither a training phase nor any prior knowledge about the morphology of heart beats in GCG/SCG signals. Remote heart rate monitoring using smartphones and mHealth apps can soon be harnessed for rhythm management and cardiovascular disease monitoring [2]. However, MCG signals tend to have interpersonal variations due to individual differences, e.g. in sensor placement, body mass index (BMI), age, sex, somatic and health conditions, resulting in vastly diverse beat morphologies. Moreover, MCG signals are susceptible to motion artefacts that can easily overshadow the rhythm signal and, thus, the quality of the recording [10], [11]. For these reasons, beat-to-beat detection from mechanical motion signals with accurate timing and amplitude information is still one of the main challenges in the analysis of these signals. Currently

M.K., M.J.T., O.L., T.H., M.P. and T.K. are with the Department of Future Technologies, Faculty of Science and Engineering, University of Turku, Finland. A.S. is with the Heart Centre, Turku University Hospital, Finland and PET Centre, Turku University hospital, Turku, Finland. This study was partially supported by Tekes (the Finnish Funding Agency for Innovation) under grant number 543/31/2015 and the Academy of Finland under grant number 290930. E-mail: mkaist@utu.fi.

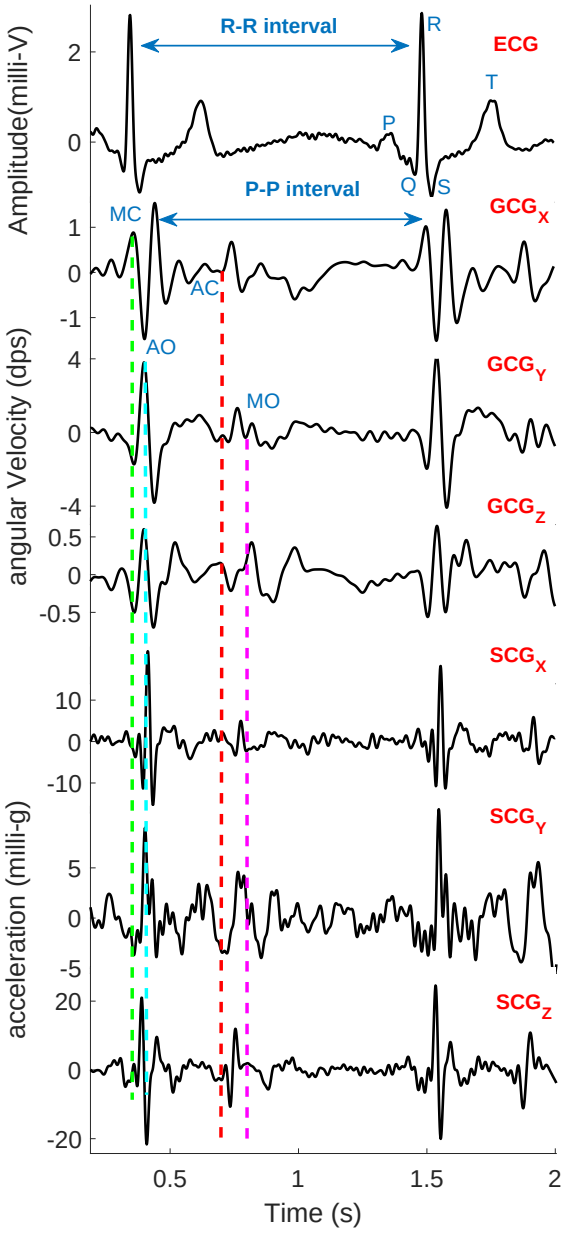

Fig. 1. Typical mechanocardiograms. SCG records accelerations of the chest wall, and GCG measures the angular velocity of micro-rotations of the chest.

available methods include wavelet transform [12], Hilbert transform [13], classification and clustering [14]–[17], merging of estimators [18], ensemble averaging [19], hidden Markov models [20], template-matching [21], regression modelling and unsupervised learning [22], pitch-tracking [23] and envelope detection and deterministic windowing [24].

In this study, a sensor modality and algorithm fusion of automatic and stand-alone (ECG-independent) heart beat detection is considered for enhanced heart beat detection. The investigation was carried out with healthy patients and those with heart disease. The algorithm selects the best signal, removes the motion artefacts, detects the beats based on the signal envelope and morphological characteristics, and finally merges the detected beat locations using both accelerometer and gyroscope signals.

This paper is organized as follows: Section II describes data acquisition. Section III provides the details of the developed algorithm, and Section IV presents the results and discussion of the presented work, followed by the concluding SectionV.

II. Data Acquisition and Collection Protocol

Seismocardiographic data were obtained by a triple-axis capacitive digital accelerometer (Freescale Semiconductor, MMA8451Q, Austin, TX, USA), while gyrocardiographic data were acquired with a three-axis angular rate (gyroscope) sensor (Maxim Integrated, MAX21000, San Jose, CA, USA). This joint embedded sensor array was configured to function as a six-degrees-of-freedom inertial measurement unit (IMU) in order to measure the cardiogenic motions of the upper chest. A two-lead electrocardiogram signal (ADS1293 from Texas Instruments) was used as a reference signal. All measurements were stored on a memory card and processed later using custom-made software. All GCG, SCG and ECG data were recorded simultaneously with a sampling frequency (F_s) of 800 Hz. All data were recorded with sensors attached to the sternum using double-sided tape. The subjects were lying either in the supine position or on their left or right side. The axes of rotations/translations were defined as follows: the x-axis points were oriented laterally from left to right (sinister–dexter), the y-axis points were directed from head to foot (superior–inferior) and the z-axis points were oriented from back to chest (dorsoventral). All the data acquisitions were performed and then processed for up to 10 min per subject. All signal post-processing and algorithm development was done in Matlab.

The study subjects for this study were divided into two groups:

Dataset I (DS I): The healthy group consisted of 29 volunteers (all male). The demographics of these subjects were as follows (min-max, mean, standard deviation): age (23–41, 29, 5 years), height (170–190, 179, 5 cm), weight (60–98, 76, 11 kg) and BMI (18–30, 24, 3.00 kg/m^2). The dataset consists of about 260 min of recordings in total.

Dataset II (DS II): The experimental group consisted of 12 patients with coronary artery disease (CAD; 10 males and 2 females) with the following demographic information: age (44–69, 57, 7 years), height (177–200, 164, 9 cm), weight (69–116, 69, 15 kg) and BMI (22.4–32.5, 28.75, 3.40 kg/m^2). The study was conducted in accordance with the Declaration of Helsinki. The study protocol was approved by the Ethical Committee of the Hospital District of South-Western Finland. The dataset consists in total of about 120 min of recordings.

III. Beat Detection Algorithm

A. Overview of the Algorithm

Mechanical motion signals suffer from movement artefacts that overshadow the cardiac beats. For this reason, the algorithm employs automatic artefact removal. The resulting signal,

however, still suffers from morphology variation, which hinders the ability to detect beats accurately. Envelope-based beat detection has been found to produce reliable detection in seismocardiograms, but such schemes fail for certain signals [13], [25]. To further enhance the detection in these methods, we combine gyroscope readings with a seismocardiogram from the IMU and detect the beats using simple envelope detection as well as another promising method, clustering, which has been shown to find beat locations accurately [14], [15].

Fig. 2 shows the main steps of the algorithm. After selecting the best axes from both accelerometer and gyroscope signals, the signals are pre-processed with a band-pass filter. From these data streams, we subsequently remove the motion artefacts. The artefact-free parts of the signals are used for beat detection. Both selected accelerometer and gyroscope signals are differentiated before applying the beat detection algorithms to make the first systolic peak more prominent. The beat detection method includes using two beat detection sub-algorithms, namely wavelet enhancement and clustering, for

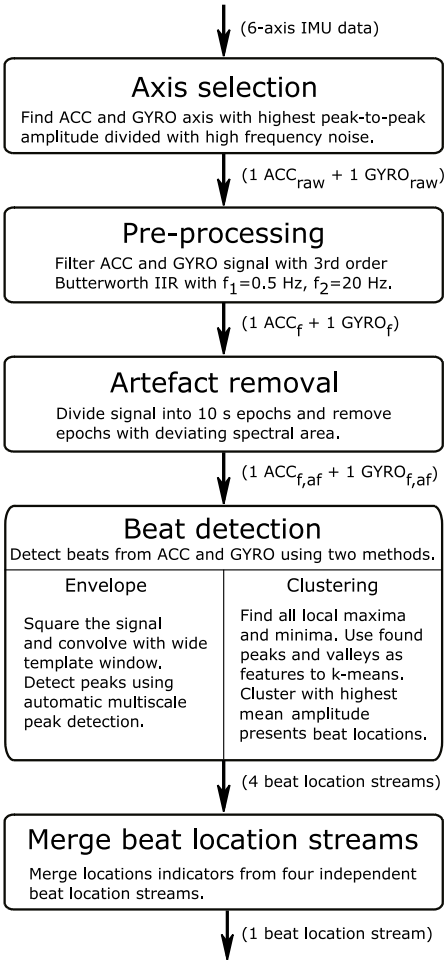

Fig. 2. Overview of the multidimensional beat-to-beat detection algorithm. The abbreviations *raw*, *f* and *af* refer to raw, filtered and artefact-free signals, respectively.

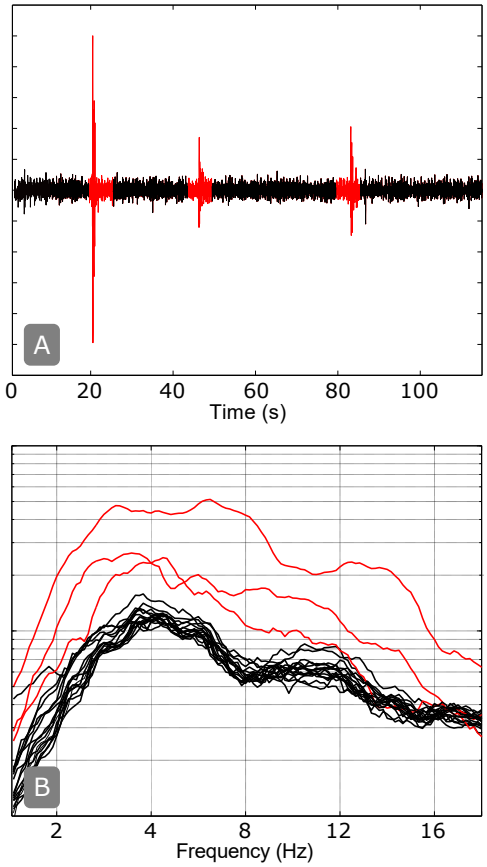

Fig. 3. A) Illustration of automatically removed artefacts (red) from an accelerometer (z-axis). B) The corresponding epoch spectra. The removed epochs (red) have clearly deviating spectra. All curves are in arbitrary units.

both accelerometer and gyroscope signals. This results in four peak candidate streams, each having their own independent candidates that are combined in the final step. This provides the final estimate on the beat positions. The steps outlined above are discussed in detail in the following sections.

B. Details of the Algorithm

First, we select the best axis from both the three-axis accelerometer and the three-axis gyroscope. The selection process is based on finding the axis that has the highest peak-to-peak amplitude divided by the absolute median deviation. The signal peak-to-peak amplitude is obtained by finding all local maximums and minimums that are separated by at least 1 s. A median is computed for both maximum and minimum streams, and the absolute difference of the medians is taken. The outcome is considered to be the signal peak-to-peak amplitude computed for each signal. The high frequency noise is obtained for the same signals by filtering them with a third-order Butterworth high-pass filter with a 50 Hz cut-off that effectively removes most of the signal information. The median absolute deviation is computed from this. The defined peak-to-peak amplitude is divided by the noise. This gives an estimate of the signal quality that is used to select the best

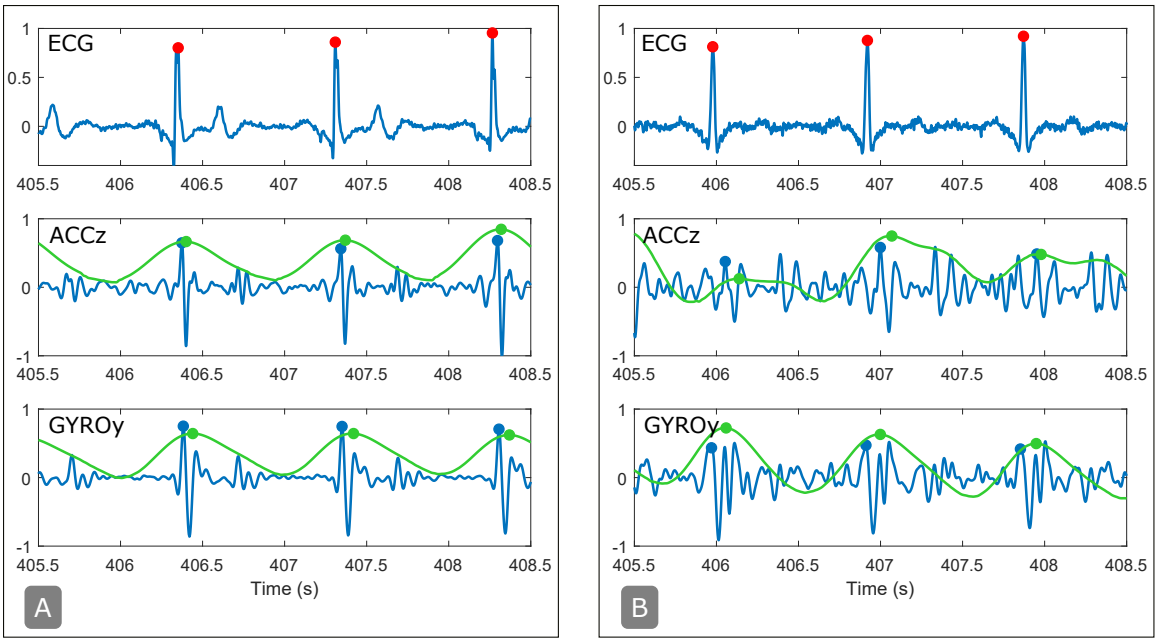

Fig. 4. Typical high-quality signal examples of A) a healthy subject and B) a coronary artery disease patient. The R-peaks in the ECG are indicated by red circles. In both accelerometer z-axis (ACCz) and gyroscope y-axis (GYROy) signals, the peaks found via clustering are indicated by blue circles in the original signal (blue,) and the peaks found in the signal envelope are indicated by green circles in the convoluted signal (green). All signals are in arbitrary units.

axis for further processing [26]. This selection is performed independently for both accelerometer and gyroscope signals with three axes. The selected signals remain unprocessed after this process.

Second, the selected original signals are filtered with a third-order Butterworth IIR filter with 0.5 and 20 Hz cut-off frequencies that remove bias, trend and high frequency noise. However, a varying degree of noise remains because the sensor is prone to pick up a significant amount of in-band noise.

Third, motion artefacts are removed from the selected signals by dividing each signal into 10-s epochs. A single-sided FFT is computed for each epoch, and the resulting spectra are smoothed with a moving average filter of 10 samples. The amplitudes within the pass-band frequency range are integrated for each epoch spectrum. Epochs with a value more than 125% of the median are removed. After each segment removal, the median value is updated, yielding a removal threshold that is always comparable and independent of the original signal quality. An example signal is shown in Fig. 3 with clear motion artefacts. In this demonstration a 6-s epochs are used. As shown, three deviating epochs were found from the accelerometer signal. Artefact removal from a gyroscope signal is not shown, but the same procedure is applied.

Heartbeats are detected independently from both accelerometer and gyroscope signals, and for both signal types, two distinct beat detection principles are used. This yields a total of four candidate peak streams. These streams are combined, resulting in the final estimate of the beat locations.

1) Envelope-Based Detection: A robust and straightforward method of peak detection is to use narrow-band filtering, which preserves information on the complex frequency of beats but omits the morphological details [25]. For this, we employ the following consecutive steps: i) sample-wise squaring to enhance peak amplitudes and ii) convolving the signal with a Gaussian-shaped template window of 800 ms. The resulting signal is much simpler in structure and resembles a signal envelope, as shown in Fig. 4. From the resulting principal signal, the candidate peaks are detected using automatic multiscale peak detection (AMPD) [27]. This algorithm constructs a scale-dependent matrix with local maximums that are used for peak detection. The details of the algorithm have already been presented [27]. Lastly, a search-back refinement process is used. For each peak candidate, there is a forward window, wf, from which the maximum amplitude is selected:

$$wf_i = (t_i + 0.4s, t_i + 1.6s). \tag{1}$$

This limits the detection between heart rates ranging from 37.5 to 150 bpm. An example of envelope-based detection is illustrated in Fig. 4.

2) Clustering-Based Detection: Unsupervised k-means clustering was used as a second beat detection method. First, all local maxima and minima are computed from the pre-processed signal. Second, the amplitudes of consecutive maxima and minima are considered to be features for the k-means clustering process. For each local maxima, feature vectors, f_a and f_g, are created for accelerometer and gyroscope signals, respectively, as follows:

$$\mathbf{f}_a = (max_i, min_i, max_{i+1}, min_{i+1}), \tag{2}$$

$$\mathbf{f}_g = (max_i, min_i, max_{i+1}). \tag{3}$$

The last minima in gyroscope signals are excluded due to their simpler waveform morphology. The measure used is squared Euclidean distance. The correct cluster is identified by finding the cluster with highest average peak amplitude.

Similarly, as described in the preceding section on the envelope approach, a search-back routine is initiated. The first peak candidate within the window (Eq. 1) is selected. An example of clustering-based detection is illustrated in Fig. 4.

3) Merging the Location Streams of of Beats: After selecting the best channel for both accelerometer and gyroscope signals and using the two-beat detection methods outlined above, we have four beat location streams. We merge these four beat candidate streams into one stream, which is the final estimate of the beat locations. The merging process follows the guidelines presented by Brüser et al. [14]. Briefly, the peak candidates found in each stream will pair to no more than one other candidate in each of the three other streams. Each candidate will pick the candidate closest to its own location, and if no pairing candidate is found within a 0.33-s window, no pairing takes place.

Then, each candidate in all four streams is assigned a quality variable by taking the absolute difference between each peak amplitude and the median amplitude of that stream. This results in each peak candidate having a quality metric associated with it. Each beat in a stream is normalized to have a maximum quality of one. The candidates that find each other from different streams have a matching location, and their quality indicators are summed together. Therefore, the quality of indicators with cross-pairing will be greatly amplified compared to those that do not. If a certain beat location is able to pair between all four streams, the maximum final quality of that beat will be four.

Finally, each detected beat is designated as either a true peak or a false one by comparing the final quality to a predetermined threshold. The threshold is manually chosen to be one, found experimentally using the DS I, and the same threshold is used in DS II. The candidates that are unable to pair with any other stream are removed. The inclusion of candidates that find only one cross-pair is determined to a large extent by the quality. The remaining candidates are mostly true peaks. The threshold can be adjusted for beat finding sensitivity, i.e. a trade-off between false positives and negatives. The final location is found by using the merged beat location as a fiducial point and by finding the maximum peak around a small window. The performance metrics are detailed in the Appendix.

C. Heart Rate Estimation

The algorithm's ability to estimate heart rate was evaluated. First, an additional refinement step [15] was carried out since each false peak significantly changes the estimated heart rate. Every beat interval was compared to the median of the previous eight beat intervals, m, and the interval ΔP_{ij} was accepted if

$$\Delta P_{ij} < 1.6 \times m \wedge \Delta P_{ij} > m/1.6, \tag{4}$$

and it was disregarded otherwise. Next, the signal was averaged with a 10-beat moving average filter before computing the average root mean square error (RMSE) between mechanical motion signals and the ECG reference signal.

TABLE I. BEAT-TO-BEAT DETECTION PERFORMANCE METRICS FOR DS I (HEALTHY SUBJECTS) USING THE PRESENTED METHOD COMPARED TO THOSE METRICS USING THE HABIT ALGORITHM [13] ON THE SAME DATASET.

	This method			HABIT	
ID	$\overline{\Delta P_{ij}}$ (ms)	TPR (%)	PPV (%)	TPR (%)	PPV (%)
1	1075	100	100	100	100
2	967	99.0	99.0	100	100
3	1136	100	100	100	99.0
4	947	100	100	100	100
5	890	100	100	97.8	98.5
6	1127	100	100	99.0	100
7	1086	100	100	98.2	100
8	815	100	100	99.6	99.6
9	976	100	100	73.3	79.3
10	834	100	100	100	100
11	956	100	100	99.9	99.8
12	972	100	98.0	100	100
13	1033	100	99.8	99.6	100
14	1178	99.3	96.6	100	95.1
15	869	100	99.5	21.0	22.0
16	934	100	100	99.1	99.4
17	1235	100	95.79	98.9	95.8
18	828	99.7	99.9	98.5	99.0
19	1053	100	100	100	100
20	999	100	100	100	100
21	876	99.7	99.7	100	100
22	770	100	100	99.2	99.2
23	972	99.7	99.7	99.8	100
24	952	100	99.7	99.8	100
25	922	99.7	100	100	100
26	937	99.8	100	99.7	100
27	748	100	100	97.7	98.9
28	1012	100	100	100	100
29	834	100	99.3	99.2	99.3
$\overline{x}$	963	99.9	99.6	95.9	96.0

TABLE II. AVERAGE BEAT-TO-BEAT DETECTION PERFORMANCE COMPARISON BETWEEN SUPINE, AND LEFT AND RIGHT LATERAL POSITIONS ON HEALTHY SUBJECTS.

	$\overline{\Delta P_{ij}}$ (ms)	TPR (%)	PPV (%)
supine (n=29)	963	99.9	99.6
left (n=6)	962	99.8	99.3
right (n=6)	952	99.3	99.0

IV. RESULTS AND DISCUSSION

The best axes for most recordings were the z-axis (dorsoventral) for accelerometer signals and the y-axis for gyroscope signals (superior–inferior). The axis-selection algorithm was able to identify the best axes in 90% and 96% percent of cases for accelerometer and gyroscope signals, respectively. These results are not surprising given that the sensor placement was carefully controlled in this study, but the results indicate that a simple selection method could be useful for remote health monitoring applications.

The removal of artefacts was designed to eliminate the deviating parts of signals, on the assumption that most parts of a signal have a stationary average spectral power. The average duration of the signals after artefact removal were 93.4% and

TABLE III. BEAT-TO-BEAT DETECTION PERFORMANCE METRICS FOR DS II (HEART DISEASE PATIENTS).

		Range: [-150 ms: +150 ms]						Range: [-100 ms: +200 ms]					
		SCG		GCG		SCG + GCG		SCG		GCG		SCG + GCG	
ID	$\overline{\Delta P_{ij}}$ (ms)	TPR (%)	PPV (%)	TPR (%)	PPV (%)	TPR (%)	PPV (%)	TPR (%)	PPV (%)	TPR (%)	PPV (%)	TPR (%)	PPV (%)
1	1069	98	96	99.2	98	98.2	97.2	99	97	99.2	98	99.2	98.2
2	992	79.3	76.7	93.6	93	78.9	78.7	99.2	96	94.9	94	99.0	98.7
3	1290	96.3	96.3	97.7	85.6	96.9	97.9	98.8	98.8	52.4	46.1	97.5	94.1
4	1039	81.7	81.6	81.4	81.3	80.2	80.2	82.2	82.1	94.2	94	80.7	80.7
5	1146	33	32.8	79.1	79.9	43.4	44.1	70.3	69.9	81.9	83.2	83.9	85.1
6	1140	66.5	64.9	100	100	75.6	75.0	76	74.1	100	100	99.1	98.5
7	1289	75.3	74.8	64.3	64.1	75.4	74.9	96.1	94.9	99.7	99.4	97.1	96.1
8	1157	29.4	29.5	90.5	90.8	31.0	31.0	97.8	97.6	99.6	100	99.1	99.1
9	1000	99.5	99.3	100	100	99.8	99.8	99.3	99.3	100	100	100	100
10	1193	74.6	73.5	99.1	94.9	80.7	79.8	98	96.3	99.1	94.9	99.8	99.5
11	1176	85.6	85	99.4	99	71.5	71.3	98.4	97.6	99	98.8	99.0	98.8
12	1347	98.7	96.9	98.2	97.6	99.1	98.0	98.7	96.9	99.3	98.7	99.1	98.0
$\overline{x}$	1153	76.5	75.6	91.9	90.3	77.6	77.3	92.8	91.7	93.3	92.3	96.1	95.6

92.6% compared to the original signal lengths for DS I and DS II, respectively, without any clear difference between the sensor modalities. This similarity in coverage, even though there are clear differences in the beat morphologies between the datasets, implies that the algorithm is robust against different study subjects.

The performance of the beat-to-beat estimation of the presented method was assessed and computed separately for each subject in both datasets using various metrics (see the Appendix). The results are collected in Tables I, II and III. In Table I, the detection performance is compared to the previously developed HABIT algorithm [13]; the same dataset (DS I) was used for both algorithms, whereas the HABIT algorithm used only seismocardiography. The true predictive rate (TPR) and positive predictive value (PPV) were 99.9% and 99.6%, respectively, in this study, and these rates showed improved performance compared to the earlier contribution [13]. The nearly perfect detection performance is largely due to high-quality data.

A further evaluation was made with subjects lying on their right and left sides. A similar detection accuracy was achieved compared to measurements in the supine position, as shown in Table II. This shows that a proper mechanical coupling between a sensor and the chest can be achieved with small, light sensing devices – although in the supine position, measurements can be carried out by simply placing the sensor on the chest.

To thoroughly evaluate the performance of the method, more challenging signals were studied from heart disease patients in a clinical environment. As illustrated in Fig. 4, the heart disease patients had different morphologies between SCG and GCG, and the systole of these patients were clearly wider than those of the healthy individuals. We evaluated the detection accuracy of the fusion approach (SCG+GCG) and compared it with individual sensing modalities, as shown in Table III. Interestingly, GCG showed the best beat detection accuracy whereas the SCG+GCG showed only marginal improvement over the use of SCG. The reason for this is that the algorithm is unable to find the correct location of an oscillating beat with a long duration, and these oscillations are more prominent in SCG. A further investigation was carried out by shifting the beat detection window (see the Appendix) by 50 ms to the following range: [-100 ms: +200 ms]. This drastically changed the obtained detection accuracies since the vast majority of the missed beats among the heart disease patients fell just outside of the detection window. This could be a result of a larger average delay between the R-peak and the mechanical response, as well as due to the long duration of systole, in comparison with the healthy subjects. With this new definition for the detection window, SCG and GCG individually showed comparable results; in contrast, the fused approach showed the best performance with the TPR and PPV at 96.9% and 95.3%, respectively.

Several clustering methods have been shown to be beneficial in detecting beats from ballistocardiograms [14], [15]. We investigated hierarchical clustering, Gaussian mixture models and k-means clustering algorithms. The inclusion of these algorithms in the fusion approach, compared to not using any clustering, showed the following average improvements in accuracy over both datasets: 1.4%, 1.8% and 1.9% for hierarchical clustering, Gaussian mixture models and k-means clustering, respectively. Although the average improvements seem moderate, the major benefit of fusing clustering with envelope detection is the ability to significantly improve some measurements that fail using envelope detection only. For example, subject 5 in DS II had an F1 score increase from 68.3% to 84.5% (not shown), indicating a clear performance improvement on a signal that had a low signal-to-noise ratio and strong diastolic peaks.

As hinted above, the beat detection accuracy does not reveal the full detection accuracy, and depending on how correct detection is defined, vastly different accuracies can be obtained. Additional performance metrics with the RMSE between beat intervals and the RMSE for the estimated heart rate (RMSE^{HR}) were computed for each subject in both datasets. These are shown in Fig. 5. The boxplots include average values for each subject and, thus, reveal how the error is distributed between different subjects, i.e. inter-subject variability. The sensor modality comparison was carried out for DS II but omitted for DS I because the high-quality

data of DS I provided a less interesting comparison. In both RMSE and RMSE^{HR}, the fusion approach showed lowest deviation between subjects, as well as lower mean values. The mean RMSE and RMSE^{HR} were 60.3 ms and 1.05 bpm, respectively, for the fused approach for DS II. The healthy subjects in DS I provided clearly smaller errors, with respective values of 5.6 ms and 0.1 bpm.

To further investigate the timing accuracy, Bland–Altman plots were generated for the correctly identified cardiac cycle intervals for both datasets using the fused approach. These plots are shown in Fig. 6. The 95% confidence intervals were (-11 ms: +11 ms) and (-113 ms: 114 ms) for DS I and DS II, respectively. There was no bias in the error in either case. The algorithm did not perform as well for the diseased group as it did with the healthy group. This is mostly likely due to the wide systole in the mechanical signals with increased oscillations, which resulted in an inaccurate estimation of the corresponding R-peak locations. This implies that rhythm monitoring with heart disease subjects is still challenging, although the algorithm was able to distinguish among the majority of the heartbeats accurately. One possible solution to better match the exact location would be to use template modelling [15]. According to the results, the CAD patients, treated with beta blockers, had slower heart rates and a non-normal distribution of cardiac cycle intervals. Further

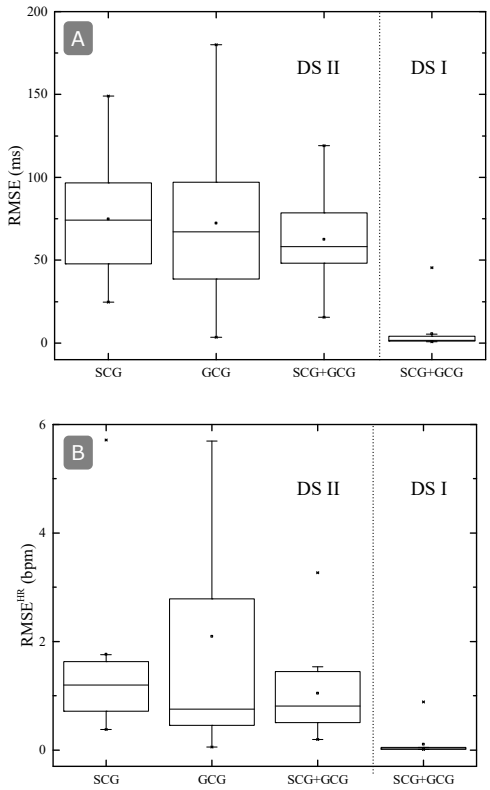

Fig. 5. Beat detection performance metrics. For each case, the rectangle spans the 1st to the 3rd quartile, where the horizontal line is the median and the dot is the mean. The whiskers present the 10% to 90% interval. Extreme values are indicated by a cross symbol.

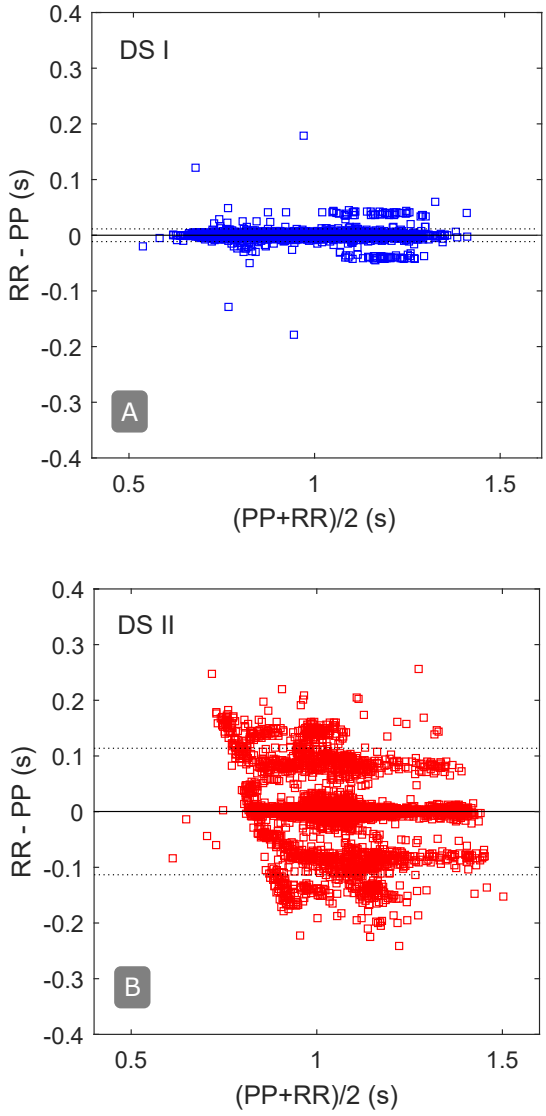

Fig. 6. Bland–Altman plots for A) the healthy group (DS I) and B) the heart disease group (DS II). The dashed lines indicate the 95% confidence interval.

investigation showed that the RR intervals in the CAD patients had a somewhat abrupt lower limit of around 0.8 s. The non-normality is probably due to the combined effect of the reduced heart rate variability in CAD patients and their beta blocker treatment [28]. In conclusion, the performance metrics show that the proposed method can measure beat-to-beat intervals in both healthy and cardiac disease subjects, while heart disease patients provide a clearly more challenging case.

V. Conclusion

We presented a stand-alone technique for heartbeat detection that benefits from fusing accelerometer and gyroscope signals. The method was able the detect beats accurately from healthy subjects and coronary artery disease patients, but timing information was clearly less accurate with heart

diseased patients due to more challenging beat morphology. A future task is to investigate a larger study group for a better understanding of the capabilities of the presented method in healthcare applications.

ACKNOWLEDGMENTS

This study was partially supported by Tekes (the Finnish Funding Agency for Innovation) under grant number 543/31/2015 and the Academy of Finland under grant number 290930.

APPENDIX

The performance of the presented algorithm was evaluated using synchronized reference electrocardiography (ECG) with respect to the detected heartbeat and interbeat intervals in gyrocardiography (GCG) and seismocardiography (SCG). We considered several statistical parameters, such as the mean value of beat-to-beat intervals, precision, sensitivity and the root mean square error (RMSE) of the estimated interbeat intervals and heart rates. We calculated the detection ability of the presented approach by assessing the precision, or positive predictive value (PPV), and sensitivity, or true positive rate (TPR), as follows:
For each $\mathrm{i} = 1, \dots M$, a detected heartbeat position, P_i, is considered

1) True positive (TP) if
$$\exists j \colon |\mathrm{P}_i - \mathrm{R}_j| \leq 150\text{ms}. \tag{5}$$
2) False positive (FP) if
$$\nexists j \colon |\mathrm{P}_i - \mathrm{R}_j| \leq 150\text{ms}. \tag{6}$$
3) False negative (FN), in which case the following condition is satisfied:
$$\nexists i \colon |\mathrm{P}_i - \mathrm{R}_j| \leq 150\text{ms}. \tag{7}$$

Based on the above parameters, the sensitivity (TPR) and precision (PPV) are calculated as follows:

$$\text{Sensitivity or TPR } (\%) = \frac{\mathrm{TP}}{\mathrm{TP} + \mathrm{FN}} \times 100, \tag{8}$$

$$\text{Precision or PPV } (\%) = \frac{\mathrm{TP}}{\mathrm{TP} + \mathrm{FP}} \times 100, \tag{9}$$

where TP represents the total number of TPs, FN represents the total number of FNs and FP represents the total number of FPs.
The RMSE between ECG and MEMS-based interbeat intervals was calculated. To compute these, we first define the jth RR interval in ECG by

$$\mathrm{RR}_j = R_{j+1} - R_j, \tag{10}$$

where R_j denotes timing of the jth R-peak. Similarly, the jth interbeat interval in SCG is obtained as

$$PP_j = P_{j+1} - P_j, \tag{11}$$

where P_{j+1} and P_j are consecutive heartbeats in either SCG or GCG signals. For each RR interval, we choose the P-P interval whose midpoint is closest to the RR interval's midpoint. For each of these corresponding intervals – here denoted by the indices j and k – we calculate the time difference as

$$d_{\text{error}} = RR_j - PP_k. \tag{12}$$

As a result, the $\mathrm{RMSE}_{a/g}$ for the total number of beat-to-beat intervals (n) is obtained as

$$\mathrm{RMSE} = \sqrt{\frac{1}{n}\sum_{i=1}^{n}(\mathrm{d}_{\text{error},i})^2}. \tag{13}$$

Similarly, the RMSE of heart rate measurements between ECG and GCG/SCG, $\mathrm{RMSE}_{a/g}$, was calculated as

$$\mathrm{RMSE}_{\mathrm{HR}} = \sqrt{\frac{1}{n}\sum_{j=1}^{n}(\mathrm{HR(ECG)}_j - \mathrm{HR(GCG/SCG)}_j)^2}, \tag{14}$$

where $\mathrm{HR(ECG)}_j$ and $\mathrm{HR(SCG/SCG)}_j$ are the jth mean heart rate obtained from the GCG/SCG and ECG signals, respectively.

REFERENCES

[1] G. V. Research, "Remote patient monitoring devices market worth 1.9 billion by 2025," 2018.

[2] J. Jaakkola, S. Jaakkola, O. Lahdenoja, T. Hurnanen, T. Koivisto, M. Pänkäälä, T. Knuutila, T. O. Kiviniemi, T. Vasankari, and K. J. Airaksinen, "Mobile phone detection of atrial fibrillation with mechanocardiography," *Circulation*, vol. 137, no. 14, pp. 1524–1527, 2018.

[3] J. Allen, "Photoplethysmography and its application in clinical physiological measurement," *Physiological Measurement*, vol. 28, no. 3, p. R1, 2007.

[4] J. W. Gordon, "Certain molar movements of the human body produced by the circulation of the blood," *Journal of Anatomy and Physiology*, vol. 11, pp. 533–536, 1877.

[5] E. C. Rubenstein, "A review of clinical ballistocardiography," *New England Journal of Medicine*, vol. 247, no. 5, pp. 166–173, 1952, pMID: 14941310.

[6] B. S. Bozhenko, "Seismocardiography– a new method in the study of functional conditions of the heart," *Terapevticheskii Arkhiv*, vol. 33, pp. 55–64, 1961.

[7] J. Zanetti and D. Salerno, "Seismocardiography: a technique for recording precordial acceleration," in *Computer-Based Medical Systems, 1991. Proceedings of the Fourth Annual IEEE Symposium*, May 1991, pp. 4–9.

[8] M. Jafari Tadi, E. Lehtonen, A. Saraste, J. Tuominen, J. Koskinen, M. Teräs, J. Airaksinen, M. Pänkäälä, and T. Koivisto, "Gyrocardiography: A new non-invasive monitoring method for the assessment of cardiac mechanics and the estimation of hemodynamic variables," *Scientific Reports*, vol. 7, no. 1, p. 6823, 7 2017. [Online]. Available: https://doi.org/10.1038/s41598-017-07248-y

[9] C. Yang and N. Tavassolian, "Combined seismo- and gyrocardiography: A more comprehensive evaluation of heart-induced chest vibrations," *IEEE Journal of Biomedical and Health Informatics*, vol. PP, no. 99, pp. 1–1, 2017.

[10] O. Inan, P.-F. Migeotte, K.-S. Park, M. Etemadi, K. Tavakolian, R. Casanella, J. Zanetti, J. Tank, I. Funtova, G. Prisk, and M. Di Rienzo, "Ballistocardiography and seismocardiography: A review of recent advances," *Biomedical and Health Informatics, IEEE Journal of*, vol. 19, no. 4, pp. 1414–1427, July 2015.

[11] J. Zanetti and K. Tavakolian, "Seismocardiography: Past, present and future," in *Engineering in Medicine and Biology Society (EMBC), 2013 35th Annual International Conference of the IEEE*, July 2013, pp. 7004–7007.

[12] C. Alvarado-Serrano, P. S. Luna-Lozano, and R. Palls-Areny, "An algorithm for beat-to-beat heart rate detection from the bcg based on the continuous spline wavelet transform," *Biomedical Signal Processing and Control*, vol. 27, pp. 96 – 102, 2016.

[13] M. J. Tadi, E. Lehtonen, T. Hurnanen, J. Koskinen, J. Eriksson, M. Pänkäälä, M. Teräs, and T. Koivisto, "A real-time approach for heart rate monitoring using a Hilbert transform in seismocardiograms," *Physiological Measurement*, vol. 37, no. 11, p. 1885, 2016.

[14] C. Bruser, K. Stadlthanner, S. de Waele, and S. Leonhardt, "Adaptive beat-to-beat heart rate estimation in ballistocardiograms," *Information Technology in Biomedicine, IEEE Transactions on*, vol. 15, no. 5, pp. 778–786, Sept 2011.

[15] J. Paalasmaa, H. Toivonen, and M. Partinen, "Adaptive heartbeat modelling for beat-to-beat heart rate measurement in ballistocardiograms," *Biomedical and Health Informatics, IEEE Journal of*, vol. PP, no. 99, pp. 1–1, 2014.

[16] F. Khosrow-khavar, K. Tavakolian, A. Blaber, J. Zanetti, R. Fazel-Rezai, and C. Menon, "Automatic annotation of seismocardiogram with high-frequency precordial accelerations," *Biomedical and Health Informatics, IEEE Journal of*, vol. 19, no. 4, pp. 1428–1434, July 2015.

[17] F. Khosrow-Khavar, K. Tavakolian, A. Blaber, and C. Menon, "Automatic and robust delineation of the fiducial points of the seismocardiogram signal for non-invasive estimation of cardiac time intervals," *IEEE Transactions on Biomedical Engineering*, vol. PP, no. 99, pp. 1–1, 2016.

[18] C. Bruser, S. Winter, and S. Leonhardt, "Robust inter-beat interval estimation in cardiac vibration signals," *Physiological Measurement*, vol. 34, no. 2, p. 123, 2013.

[19] C. Yang, S. Tang, and N. Tavassolian, "Utilizing gyroscopes towards the automatic annotation of seismocardiograms," *IEEE Sensors Journal*, vol. 17, no. 7, pp. 2129–2136, April 2017.

[20] J. Wahlstrom, I. Skog, P. Handel, F. Khosrow-khavar, K. Tavakolian, P. K. Stein, and A. Nehorai, "A Hidden Markov Model for Seismocardiography," *IEEE Transactions on Biomedical Engineering*, vol. PP, no. 99, pp. 1–1, 2017.

[21] J. H. Shin, B. H. Choi, Y. G. Lim, D. U. Jeong, and K. S. Park, "Automatic ballistocardiogram (bcg) beat detection using a template matching approach," in *Engineering in Medicine and Biology Society, 2008. EMBS 2008. 30th Annual International Conference of the IEEE*, Aug 2008, pp. 1144–1146.

[22] H. Ashouri and O. T. Inan, "Automatic detection of seismocardiogram sensor misplacement for robust pre-ejection period estimation in unsupervised settings," *IEEE Sensors Journal*, vol. 17, no. 12, pp. 3805–3813, June 2017.

[23] M. D. Zink, C. Brüser, B.-O. Stüben, A. Napp, R. Stöhr, S. Leonhardt, N. Marx, K. Mischke, J. B. Schulz, and J. Schiefer, "Unobtrusive nocturnal heartbeat monitoring by a ballistocardiographic sensor in patients with sleep disordered breathing," *Scientific Reports*, vol. 7, no. 1, p. 13175, 2017.

[24] M. Di Rienzo, E. Vaini, and P. Lombardi, "An algorithm for the beat-to-beat assessment of cardiac mechanics during sleep on earth and in microgravity from the seismocardiogram," *Scientific Reports*, vol. 7, no. 1, p. 15634, 2017.

[25] T. Hurnanen, M. Kaisti, M. J. Tadi, M. Vähä-Heikkilä, S. Nieminen, Z. Iftikhar, M. Paukkunen, M. Pänkäälä, and T. Koivisto, *Heartbeat Detection Using Multidimensional Cardiac Motion Signals and Dynamic Balancing*. Singapore: Springer Singapore, 2018, pp. 896–899.

[26] M. Kaisti, J. Leppanen, O. Lahdenoja, P. Kostiainen, M. Pänkäälä, U. Meriheina, and T. Koivisto, "Wearable pressure sensor array for health monitoring," in *Computing in Cardiology 2017 (CinC), Rennes, France*, 2017.

[27] F. Scholkmann, J. Boss, and M. Wolf, "An efficient algorithm for automatic peak detection in noisy periodic and quasi-periodic signals," *Algorithms*, vol. 5, no. 4, pp. 588–603, 2012.

[28] M. J. Niemelä, K. Airaksinen, and H. V. Huikuri, "Effect of beta-blockade on heart rate variability in patients with coronary artery disease," *Journal of the American College of Cardiology*, vol. 23, no. 6, pp. 1370 – 1377, 1994.